Journal of
Applied Crystallography
ISSN 0021-8898

Received 24 July 2000
Accepted 20 November 2000

Characterization of H defects in the aluminium–hydrogen system using small-angle scattering techniques

C. E. Buckley,[a]* H. K. Birnbaum,[b] J. S. Lin,[c] S. Spooner,[c] D. Bellmann,[d] P. Staron,[d] T. J. Udovic[e] and E. Hollar[b]

[a]Department of Applied Physics, Curtin University of Technology, GPO Box U 1987, Perth 6845, WA, Australia, [b]Materials Research Laboratory, University of Illinois, Urbana, Il 61801, USA, [c]Oak Ridge National Laboratory, Solid State Division, Oak Ridge, TN, USA, [d]Institute for Materials Research, GKSS-Research Centre Geesthacht GmbH, D-21502 Geesthacht, Germany, and [e]NIST Center for Neutron Research, National Institute of Standards and Technology, 100 Bureau Dr., MS 8562, Gaithersburg, MD 20899-8562, USA. Correspondence e-mail: rbuckley@cc.curtin.edu.au.

Aluminium foils (99.99% purity) and single crystals (99.999% purity) were charged with hydrogen using a gas plasma method and electrochemical methods, resulting in the introduction of a large amount of hydrogen. X-ray diffraction measurements indicated that within experimental error there was a zero change in lattice parameter after plasma charging. This result is contradictory to almost all other face-centred cubic (f.c.c.) materials, which exhibit a lattice expansion when the hydrogen enters the lattice interstitially. It is hypothesized that the hydrogen does not enter the lattice as an interstitial solute, but instead forms an H–vacancy complex at the surface that diffuses into the volume and then clusters to form H_2 bubbles. Small- and ultra-small-angle neutron scattering (SANS, USANS) and small-angle X-ray scattering (SAXS) were primarily employed to study the nature and agglomeration of the H–vacancy complexes in the Al–H system. The SAXS results were ambiguous owing to double Bragg scattering, but the SANS and USANS investigation, coupled with results from inelastic neutron scattering, and transmission and scanning electron microscopy, revealed the existence of a large size distribution of hydrogen bubbles on the surface and in the bulk of the Al–H system. The relative change in lattice parameter is calculated from the pressure in a bubble of average volume and is compared with the experimentally determined value.

1. Introduction

Although studies of the solubility of hydrogen in molten and solid aluminium in the temperature range 573–1473 K (Ransley & Neufeld, 1948; Ichimura *et al.*, 1988; Lin & Hoch, 1989; Ichimura *et al.*, 1992; Ichimura & Sasajima, 1993) have been carried out, little is known of the solubility of hydrogen in aluminium at room temperature. The diffusivity and permeability of hydrogen in aluminium has been studied in the temperature range 285–328 K (Ishikawa & Mclellan, 1986), but no independent measurement of the solubility was made. Recent measurements of the solubility of hydrogen in aluminium (Birnbaum *et al.*, 1997) at room temperature showed that very large concentrations [>1000 atomic parts per million (a.p.p.m.)] of hydrogen were introduced into the aluminium matrix using electrochemical, chemical and ultrasonic water-bath charging techniques. However, it has since been demonstrated that owing to the formation of an $Al(OH)_3$ layer on the surface of the Al during the cathodic and chemical charging procedure, the concentration of H in the bulk is <800 a.p.p.m. (Buckley & Birnbaum, 2000). It was shown that accurate measurements of the H concentration in the cathodically and chemically charged samples are only obtained after careful cleaning of the Al surface after charging. In the present paper, the state of H in Al is investigated using a variety of complementary techniques. To avoid spurious concentration measurements, a hydrogen gas plasma charging method was used to introduce H into Al, resulting in concentrations of up to 3000 a.p.p.m. H concentrations were measured using gas extraction and prompt gamma activation analysis (PGAA) (Lindstrom, 1993). X-ray diffraction showed that within experimental error the introduction of H into the Al matrix results in a zero change in lattice parameter, in contrast to other f.c.c. metals, where a lattice expansion of approximately 2.9×10^{-3} nm^3 per H atom is exhibited (Peisl, 1978). The structural aspects of H were investigated using small-angle X-ray scattering (SAXS), which suggested either scattering from platelet-shaped inhomogeneities (Birnbaum *et al.*, 1997) or double Bragg scattering (DBS). To resolve the ambiguity, small-angle neutron scattering (SANS) experi-

ments were carried out at wavelengths such that DBS could not occur. Further experiments using ultra-small-angle neutron scattering (USANS), transmission and scanning electron microscopy (TEM and SEM), inelastic neutron scattering (INS) and precision density measurements, revealed the existence of a large size distribution of H_2 bubbles in the plasma-charged samples (Buckley & Birnbaum, 1998). These results are discussed in terms of the mechanism of H entry and clustering in Al.

A method for calculating the relative change in lattice parameter from the SANS and USANS data is presented. In this method, the bubbles are assumed to be spherical and the relative change in lattice parameter is determined from the calculated values of the pressure in a bubble of average volume and the volume concentration of bubbles (Hirth & Lothe, 1968). Since the experimentally determined relative change in lattice parameter is an average value, our method uses an expression for the average volume of the bubbles to determine the pressure and the relative change in lattice parameter. Good agreement is obtained between the calculated and experimentally determined values for the volume concentration of bubbles and the relative change in lattice parameter. The analysis also calculates the number of vacancies per H atom created by the initial 1 keV ions.

2. Experimental

A variety of experimental techniques were used to study the H concentration and structure in Al. While the specimen requirements for each technique precluded using identical specimens for all measurements, every attempt was made to ensure comparable H concentrations and distributions for all of the techniques used. Possible loss of H and changes in the distribution were considered since the time scale and specimen procedure differed for the various techniques. Repeated H concentration measurements showed that there was no loss of H from the Al over the time periods needed for the various experiments. It was not possible to make a direct determination of whether the H distribution changed over this time period, but considerations based on the diffusivity of Al and experience from other defect studies suggest that there should be no change in distribution at room temperature.

For the SAXS experiments, specimens were cut from single crystals grown from the 99.999% aluminium in vacuum by a Bridgman technique. Prior to charging, the single crystals were oriented using a conventional back-reflection Laue X-ray technique, such that their faces were oriented parallel to the crystallographic ⟨110⟩ normals. The crystals were then cut by spark erosion, followed by polishing to a thickness of ∼70 μm. All specimens were given a final anneal at 833 K in a vacuum of 10^{-4} Pa. Several of these specimens were set aside as reference samples (not hydrided). The remaining specimens were then electrolytically charged with H using current densities in the range 0.5–50 mA cm^{-2}. The H concentration was measured on identical samples charged in parallel with the samples used for SAXS measurements (Birnbaum *et al.*, 1997).

The SAXS experiments were performed at the Center for Small Angle X-ray Scattering Research (CSASR) at the Oak Ridge National Laboratory (Wignall *et al.*, 1990) using a well-collimated Cu $K\alpha$ beam, 2.0 mm in diameter at the sample position. Scattered beams were detected by a 20 × 20 cm area detector at a distance of 5.119 m from the specimen, resulting in a resolution of 6.25×10^{-4} radians. The samples were mounted on a three-axis goniometer, allowing the scattering from H–vacancy platelets habitating the {111} or {112} planes to be studied as a function of tilt angle. The data were corrected for the detector background using empty chamber runs and for non-uniform sensitivity using ^{55}Fe standards. The corrected data were converted to absolute intensity using a pre-calibrated secondary standard of cross-linked polyethylene, provided by CSASR (Russell *et al.*, 1988).

For the neutron scattering and electron microscopy experiments, polycrystalline Al foils of 99.99% purity and ∼130 μm thickness (foil sets A, B and C) and foils of 98.6% purity and ∼50 μm thickness (foil set D), were annealed for 24 h in a vacuum of 10^{-4} Pa at 833 K. Reference samples (not hydrided) for foil sets A, B, C and D were kept aside. The remaining foils from sets A, B, C and D were then charged with H at room temperature for 72 (A), 76 (B), 78 (C) and 25 h (D) using an H_2 plasma charging technique with acceleration voltages ranging from 1 to 1.2 keV and current densities of 0.66 (A), 0.68 (B), 0.81 (C) and 0.58 mA cm^{-2} (D). Plasma charging was used instead of electrolytic charging to avoid $Al(OH)_3$ forming on the surface during charging (Buckley & Birnbaum, 2000). The H concentrations for the four sets of foils were determined by PGAA and gas chromatography to be 2500 (A), 2100 (B), 2880 (C) and 2500 (±50) a.p.p.m. (D). The integrated number of protons impinging on foil B during the plasma charging was 1.41×10^{21} cm^{-2}. Given that the concentration of H atoms in foil B was 2.1×10^{-3}, only 0.12% of the protons diffused into the bulk. The distribution of the H and the point defects created by 1 keV H^+ ions impinging on the Al foil were calculated using the *TRIM* code (Ziegler *et al.*, 1985). The average depth of the implanted H ions and the point defects created by the H ions was found to be ∼19.4 nm (see Fig. 1), which is 0.015% of the specimen thickness. The same *TRIM* code was used to calculate the depth distribution of vacancies introduced by the plasma charging.

Lattice parameter measurements were made after charging foils C and D, and on reference samples from foil sets C and D, using step scans of the X-ray peaks obtained with Cu $K\alpha$ radiation. Since the polycrystalline foils were highly textured, only one peak appeared in the diffraction data and hence the lattice parameter was calculated from the 400 reflection with the precision in $\delta a/a_0$ estimated to be 5×10^{-5}. The precision was calculated by making repeated measurements on a control specimen (including insertion in the specimen holder) and calculating the standard deviation of the measurements.

The SANS experiments were conducted on foil set B and reference samples utilizing the 30 m SANS instrument at the National Institute of Standards and Technology (NIST) Centre for Neutron Research (NCNR), using a wavelength of 0.8 ± 0.15 nm and three sample-to-detector distances (SDD):

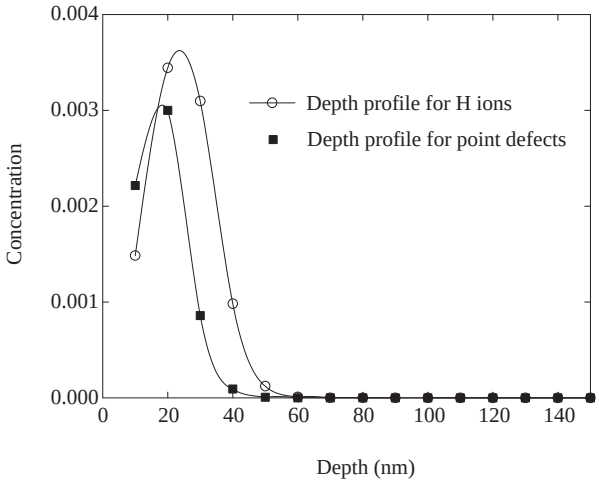

Figure 1
Depth profile of hydrogen and point defects implanted and created by H ions on an aluminium target at an accelerating voltage of 1 keV, calculated using the *TRIM* code (Ziegler *et al.*, 1985).

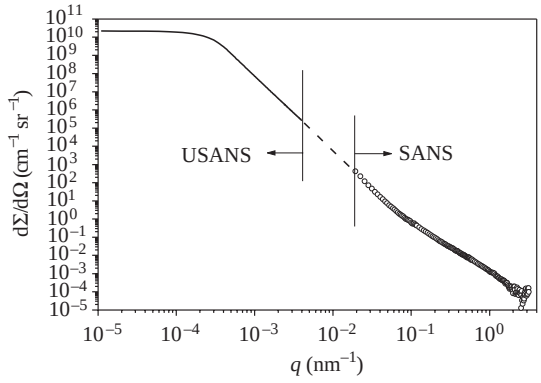

Figure 2
The differential small-angle scattering cross section over a wide q range as a result of SANS (circles) and USANS measurements. The dashed lines indicate the q region where no data were collected. For both sets of data, the experimental errors arise from the statistical errors of the measured intensities. The errors are ∼1% at low q and ∼10% at high q for the USANS data and ∼5% in the low-q region of the SANS data. Within experimental error there is excellent agreement between the low-q region of the SANS data and the high-q region of the USANS measurements.

1.3, 4.5 and 13.17 m (Buckley & Birnbaum, 1998). DBS is not possible in Al at this wavelength, since the cut-off wavelength $\lambda_c = 2d_{\max}$ is ∼0.47 nm, where $d_{\max}$ is the largest spacing between lattice planes. The intensity $I(q)$ was measured over the q range $0.019 < q\ (\mathrm{nm}^{-1}) < 3.2$, where $q = 4\pi\sin\theta/\lambda$. Ultra-small-angle neutron scattering (USANS) was performed on foil set B and reference samples at the double crystal diffractometer (DCD) at the Geesthacht Neutron Facility (GeNF) (Bellmann *et al.*, 1998) using a wavelength of 0.44244 ± 0.00036 nm. The absolute neutron wavelength of the DCD is determined by rocking a graphite crystal with a mosaic spread of 0.8° through the beam at the sample position. The resolution of the DCD is determined by the Darwin width of Si crystals, resulting in $\Delta\lambda/\lambda$ = 0.0018%. This value is very small compared to the SANS wavelength resolution, which depends upon the velocity selector helical slot dimensions. Since the wavelength used in the USANS experiment is very close to λ_c (λ_c = 0.47 nm for Al), DBS is expected to be negligible. The scattering vector range was $1.0 \times 10^{-5} \leq q\ (\mathrm{nm}^{-1}) \leq 4.0 \times 10^{-3}$, but since the range $1 \times 10^{-5} \leq q\ (\mathrm{nm}^{-1}) \leq 1.3 \times 10^{-4}$ includes overlapping of the scattering with the primary beam, $q_{\min} \simeq 1.3 \times 10^{-4}\ \mathrm{nm}^{-1}$. There is a q region ($q = 4.0 \times 10^{-3}$ to $1.94 \times 10^{-2}\ \mathrm{nm}^{-1}$) where neither SANS nor DCD data were collected (broken line in Fig. 2), as this q region was not accessible because of insufficient scattering intensity at higher q values (DCD) and the limitations of the SANS experimental setup at lower q values. However, the DCD data cannot simply be linked to the SANS data, because DCD data are slit-height smeared, while SANS is measured using a point-like collimation. Therefore, the DCD data are fitted (solid line in Fig. 3) independently of the SANS data, on the basis of a size distribution of spherical particles. The fitting procedure (Staron & Bellmann, 2001) accounts not only for the smearing caused by the DCD primary beam, but also for multiple small-angle scattering (Schelten & Schmatz, 1980). The results of the fitting procedure are the size distribution (inset in Fig. 3) and the corresponding unsmeared scattering cross section (solid line in Fig. 2). Since the SANS and USANS experiments were conducted several months apart, the stability of the H in foil B was checked following the USANS experiment by measuring the

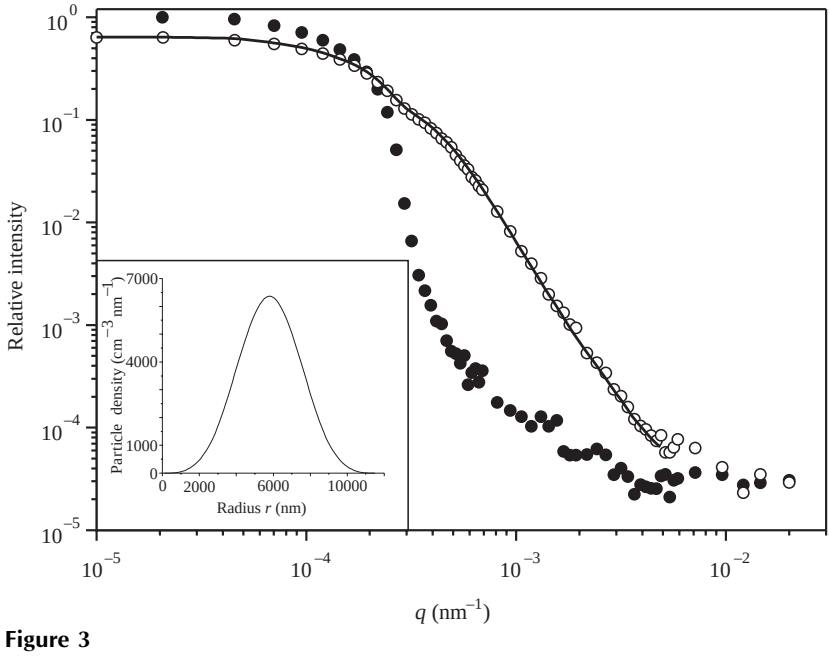

Figure 3
DCD measurements: filled circles represent the rocking curve of the empty beam, open circles represent the scattering curve from the Al–H foil (d = 260 μm), the line is the scattering curve calculated from a particle size distribution shown in the inset. The reference sample showed no scattering effect compared with the rocking curve of the empty beam.

H concentration using the PGAA method. It was found that the concentration of H in the foil was comparable with the quantity originally measured (2100 ± 50 a.p.p.m.).

Inelastic neutron scattering (INS) measurements were performed on 22.5 g of foil D and ~4.5 g of foil B, and reference samples of foils B and D, using the Fermi-chopper time-of-flight spectrometer (Copley & Udovic, 1993) at the NCNR, with an incident neutron wavelength of 0.48 nm. Sample temperature was regulated using a top-loading liquid-He-cooled cryostat.

TEM and SEM images of foil A and reference samples were taken on a Phillips 420 TEM with an operating voltage of 120 keV, and a Hitachi S 800 field emission SEM at The Materials Research Laboratory, University of Illinois. SEM specimens required no preparation, while TEM samples were electrochemically thinned in a solution of 5% perchloric acid and 95% methanol.

Precision density measurements were conducted on foil B and a reference sample using a standard four-digit balance with a precision of 0.1 mg, yielding a density precision of 0.01.

3. Results and discussion

The two-dimensional SAXS measurements from a high-purity single crystal of Al that was cathodically charged with H were highly anisotropic (streaks in the ⟨111⟩ or ⟨112⟩ directions), which is indicative of scattering from a platelet-shaped inhomogeneity or from DBS (see Fig. 4). This type of scattering could arise from platelet-shaped H–vacancy complexes habitating the {111} or {112} plane. In an effort to differentiate between DBS and scattering from plates, the crystal was oriented perpendicular to the [110] direction and tilting experiments were conducted to find the orientation that maximized the magnitude of the streaks on the scattering pattern. An f.c.c. crystal oriented perpendicular to the [110] direction will not produce DBS, but tilting of the crystal by >2° could excite a Bragg reflection and hence at certain tilt angles DBS may occur. The situation is further complicated by the fact that the primary DBS directions are also ⟨111⟩. The directions of the DBS for the experimental tilt angles were calculated and these were compared with the experimental scattering pattern.

SAXS was also conducted on reference samples (not hydrided). Some reference samples exhibited isotropic patterns, whereas other reference samples exhibited one or two streaks, the appearance of which was dependent on the tilt angle of the goniometer. Other hydrided samples exhibited isotropic scattering patterns as well as patterns exhibiting one, two, three, four, five and six streaks per pattern. The appearance of the streaks was also dependent on the tilt angle of the goniometer. The results from both the reference and hydrided samples showed enough ambiguity to suggest the need for an experiment in which the DBS would be definitively eliminated.

DBS cannot occur if the wavelength is larger than the Bragg cut-off wavelength, ($\lambda > \lambda_c$); this was utilized in SANS experiments conducted using $\lambda = 0.8 \pm 0.15$ nm. SANS was conducted on reference (not hydrided) and hydrided samples of foil set B, and the cross sections ($d\Sigma/d\Omega$) for the reference sample were subtracted from the cross sections for the hydrided samples. Since foil set B is a polycrystalline sample, the SANS results recorded on an area detector for both the reference and the hydrided foils were radially symmetric around the primary beam. Fig. 5 shows a log–log SANS plot of $d\Sigma/d\Omega$ *versus* q over the experimental q range of the data for the reference sample and the hydrided sample, with the reference-sample cross sections subtracted. It is clear that the cross sections for the hydrided sample are at least an order of magnitude larger than the reference-sample cross sections, indicating excess scattering from particles in the bulk of the hydrided sample that are not present in the reference sample. The two slopes drawn through the data for the hydrided sample indicate scattering from a wide distribution of particle sizes. Since a slope of −2 is indicative of scattering from platelet shapes, the slope of −2.75 over most of the q range suggests that the scattering is not from plates, but rather from either a very broad distribution of cluster sizes (approximately spherical) or from fractal-shaped clusters. The slope of −4.27 at small q is indicative of scattering from particles up to several micrometres in size (Buckley & Birnbaum, 1998). The q range of the SANS data, coupled with the upturn in slope at low q, is indicative of scattering from particles ranging in size from <2 nm up to several micrometres. Although there is a large

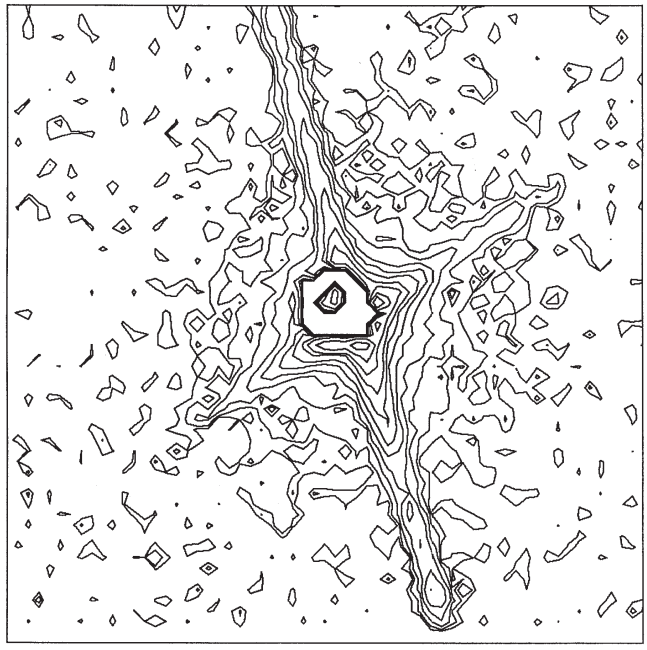

Figure 4
Two-dimensional SAXS pattern (lines of equal count rates are shown in the range of 1 to 10^3 s^{-1}) for a high-purity single crystal of aluminium electrolytically charged with hydrogen to an average concentration of ~1000 a.p.p.m.. The horizontal axis is q_x and the vertical axis is q_y. The highly anisotropic streaks in the ⟨111⟩ or ⟨112⟩ directions are indicative of scattering from a platelet-shaped inhomogeneity or from double Bragg scattering (DBS).

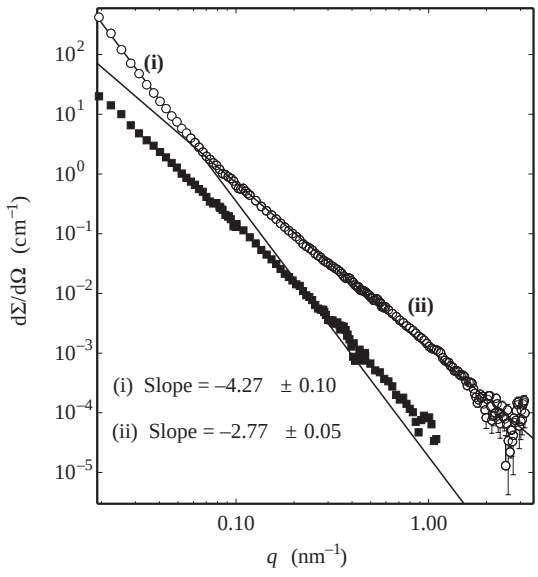

Figure 5
SANS differential scattering cross sections (dΣ/dΩ for the reference sample subtracted) for the hydrided foil B (circles) and reference foil B (squares). Two distinct slopes over (i) the low-q region and (ii) the rest of the scattering curve are shown for the hydrided foil. See text for discussion concerning the two slopes.

spread of intensities at high q, a slope of -4 is not obtained at high q; therefore, the standard Porod (1951) analysis cannot be applied to the high-q region of the scattering curve. Evidence from SEM, TEM and INS (see Figs. 6–11) supports the conclusion from the SANS results that the scattering is *not* from platelet-shaped inhomogeneities.

Evidence for scattering from particles in the size range of the order of micrometres is seen in the DCD measurement (Fig. 3). The solid line in Fig. 2 is the cross section resulting from a fit of the DCD data (solid line in Fig. 3). The resulting size distribution for the DCD measurement is based on cubic B-splines with $\langle R \rangle$ = 5800 nm, full width at half-maximum (FWHM) = 4120 nm and a volume fraction of 3.8%. Cubic B-spline functions are chosen because these functions are exactly zero at the limits of a definite interval. For both the SANS and USANS data, the experimental errors arise from the statistical errors of the measured intensities. The errors are ∼1% at low q and ∼10% at high q for the USANS data, and ∼5% in the low-q region of the SANS data. Note the excellent agreement between the SANS cross section and the scattering cross section derived from the DCD data. The USANS results can be interpreted on the basis of scattering from particles with radii in the range $0.8 \leq r$ (μm) ≤ 12.1 [$4 \times 10^{-3} \leq q$ (nm^{-1}) $\leq 1.3 \times 10^{-4}$]. Some additional scattering may arise from the rough surface of the Al foils caused by the charging process. The USANS technique does not distinguish between scattering particles in the bulk and scattering particles on the surface, since it is the same scattering process. In contrast to the hydrided foils, the reference Al foils, which have a clean surface structure, showed no additional scattering compared with the rocking curve of the empty beam.

X-ray diffraction conducted on foils C and D indicated a small lattice contraction (foil D) and expansion (foil C), but the magnitudes of these are within experimental error. The texture of the Al foils will not affect the relative change in lattice parameter, but will affect the precision with which it can be measured. The precision in $\delta a/a_0$ was estimated to be 5×10^{-5} by calculating the standard deviation of repeated measurements on a control specimen. Within experimental error, $\delta a/a_0$ values for foils C and D are equal to zero, while Table 1 shows that measurable lattice expansion would result if H, at the concentrations measured, entered the lattice interstitially. The zero change in lattice parameter is in contrast to other hydrided f.c.c. elements, which normally exhibit an expansion of 2.9×10^{-3} nm^3 per H atom (Peisl, 1978). The zero change in lattice parameter suggests that H does not enter the lattice interstitially, but instead forms H–vacancy complexes at the surface and then diffuses into the volume.

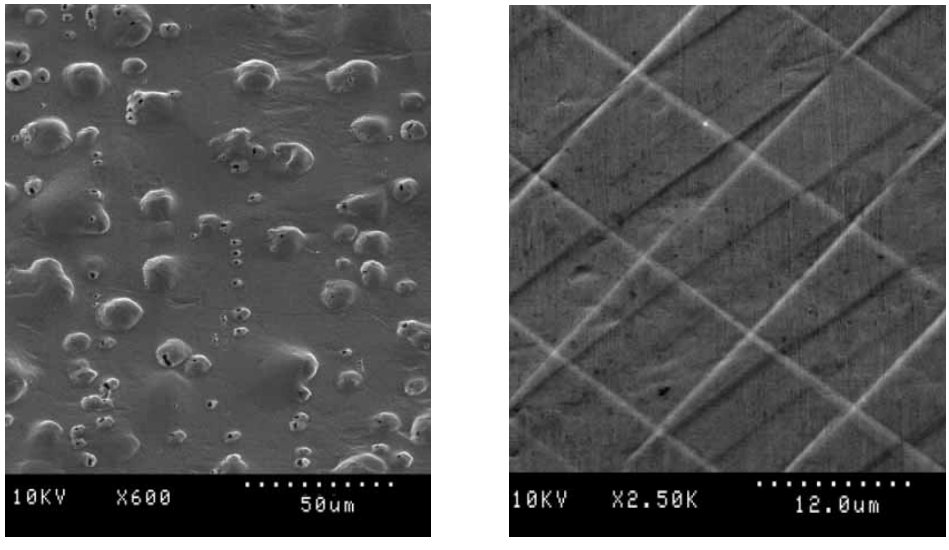

Figure 6
SEM image of foil A (C_H = 2500 a.p.p.m.) showing a range of bubble sizes on the surface, compared with that of a control sample (not hydrided), which shows no evidence of bubbles on the surface.

Microscopic examination using SEM and TEM techniques revealed the existence of large vacancy clusters, *i.e.* bubbles, at the surface, as well as in the interior (see Figs. 6 and 7). The features were identified as bubbles from the observation that the surface depressions in the SEM images often had 'lids' and that some of these 'lids' were ruptured by the internal pressure of the bubbles. The small bubbles in the TEM images were identified as such from studies of the fringe contrast in the case of isolated bubbles. The density of bubbles in the TEM images appears higher than the actual density as a result of overlap of images in the projected view characteristic of TEM images. The large size distri-

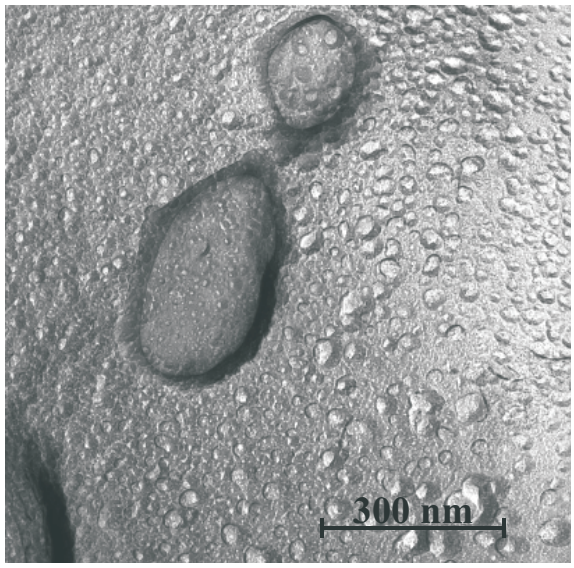

Figure 7
TEM image of foil A showing bubbles with radii in the range from 3 to 170 nm.

bution and the variability of the density from region to region precluded any detailed study of the size distribution from the SEM and TEM images. The features seen in Figs. 6, 7 and 8 are similar to those seen by other TEM, SEM and optical microscopy investigations of H implantation in Al (Kamada *et al.*, 1987, 1988; Kamada, 1989; Wei *et al.*, 1987; Milacek *et al.*, 1968). The TEM image in Fig. 7 shows a region where the bubbles are densely packed, whereas Fig. 8 shows a region containing only two bubbles with radii of ∼250 nm and 3 μm. Fig. 9 is an SEM image of foil A (H concentration C_H = 2500 a.p.p.m.), which has been electrochemically thinned to a

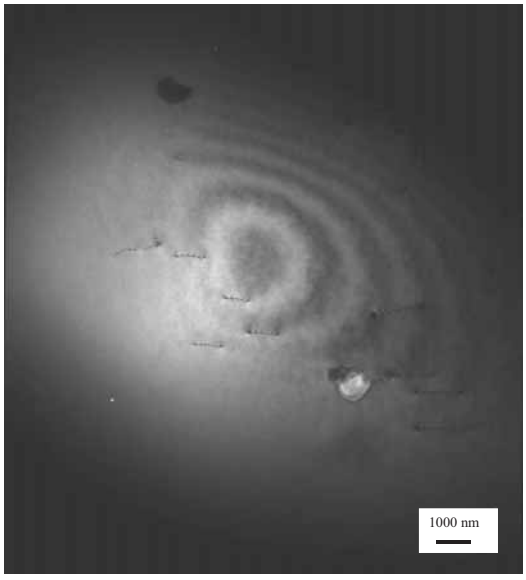

Figure 8
TEM micrograph of foil A (C_H = 2500 a.p.p.m.) showing a large and a smaller bubble with radii of ∼3 μm and 250 nm, respectively. There are no heavily dislocated regions, which suggests that H does not enter the Al lattice interstitially, but instead couples to vacancies to form H–vacancy complexes, which then cluster to form H_2 bubbles. Magnification 18500×.

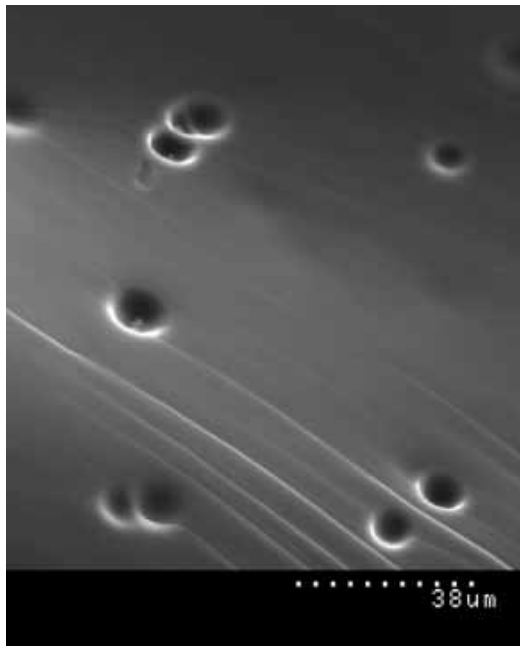

Figure 9
SEM image of an electrochemically thinned sample of foil A (C_H = 2500 a.p.p.m.). The surface of this image is approximately in the centre of the foil of thickness 130 μm. The craters on the surface of the thinned area represent large bubbles in the bulk that have had their 'lids' removed during the thinning process. This image indicates that micrometre-size bubbles are present in the bulk of the sample.

thickness of 100–500 nm. This view of the interior of the specimen shows that the bubbles seen on the surface of an H-charged specimen are present in the interior of the specimen (*i.e.* ∼65 μm from the irradiated surface) and that these bubbles have had their lids removed during the thinning process. The presence of bubbles in the region being thinned to electron transparency resulted in multiple holes bounded by little or no electron-transparent volume. In contrast, the control samples only formed one hole, which was bounded by an abundance of electron-transparent volume. This can be seen in Fig. 10, which shows a hydrided sample with several holes approximately 5–20 μm in diameter and a control sample (not hydrided) with only one hole formed during the thinning process. This behaviour was characteristic of all charged and uncharged specimens examined. None of the features visible in Figs. 7, 8 and 9 was seen in the control samples. The SEM and TEM studies clearly show that the H is inhomogeneously distributed throughout the volume of the sample and that there is a very large range of bubble sizes in the bulk of hydrided Al.

None of the TEM images of the bubbles showed any significant generation of dislocations in the vicinity of the bubbles as might be expected if the volume increase caused by the formation of the bubbles was accommodated by plastic deformation. The absence of a high dislocation density in the vicinity of the bubbles suggests that the volume increase needed to form them is not obtained by plastic processes but rather by a diffusion mechanism. Since it is expected that the interstitial H enters as a part of a vacancy cluster (Buckley &

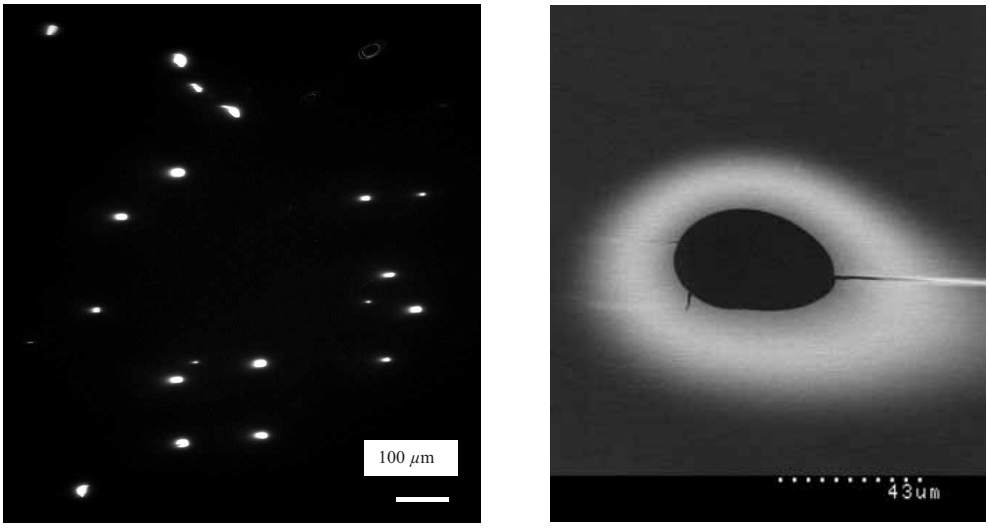

Figure 10
Low-magnification TEM images of a region of foil A, which has been hydrided (image on left) and a reference sample of foil A (image on right). The hydrided sample has formed several holes, approximately 5–20 μm in diameter, during the thinning process, whereas the reference sample (not hydrided) has only formed *one* hole during the thinning process. The hydrided sample forms several holes during the thinning process because several large bubbles have their 'lids' chopped off almost simultaneously. The reference sample only forms one hole because it has no bubbles in its bulk. Several reference samples and hydrided samples were subjected to the thinning process and in *all* cases the above behaviour occurred.

Birnbaum, 1998), it appears that the vacancies agglomerate to form the bubbles inside which the H 'precipitates' as H_2. This process is driven by the decrease in enthalpy from the annihilation of the vacancies and from the solid-solution enthalpy of interstitial H.

Inelastic neutron scattering (INS) experiments were carried out to determine the form of the H in the Al. These studies show that H is in the form of H_2 molecules, as seen from the neutron time-of-flight spectrum of 2500 a.p.p.m. H in Al at T = 6 K shown in Fig. 11. The prominent feature near 14 meV is characteristic of the *ortho*-to-*para* rotational transition of solid molecular H, and the smaller feature near 8 meV is caused by the solid H_2 translational modes. The elastic peak resolution is 0.14 meV FWHM, and at high-energy gains the resolution increases linearly with energy, resulting in a resolution of ∼1 meV FWHM at 14 meV neutron energy gain. The spectra at higher temperatures are indicative of the phase change from solid H_2 to liquid H_2. The majority, if not all of the hydrogen signal in the elastic peak (after correcting for the contribution from Al scattering) becomes quasielastically broadened when the solid H_2 transforms into a liquid between 6 and 30 K. This dramatic quasi-elastic broadening (especially at higher q) is caused by translational diffusion in the liquid H_2 phase. If chemisorbed or physisorbed H atoms were present in significant amounts, we would clearly see a sharp elastic component (because the absorbed H atoms would be essentially immobilized at these low temperatures) arising from the non-diffusing fraction of H. We do not see any significant amount of such a sharp component. Therefore, the behaviour of the elastically scattered neutron peak in the temperature range T = 6–30 K is consistent with most if not all H being trapped in the Al matrix as molecular H_2. The measurements did not cover the higher energy-transfer range in which Al–H normal-mode vibrations resulting from the possible presence of some monatomically bound H atoms would be observed. A measurement to help determine a more precise lower limit on the amount of monatomic H present will be conducted in the near future.

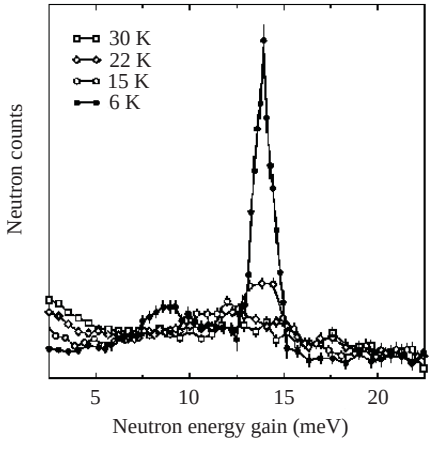

Figure 11
The neutron time-of-flight spectrum of 2500 a.p.p.m. H in aluminium at T = 6, 15, 22 and 30 K. The prominent feature near 14 meV is characteristic of the *ortho*-to-*para* rotational transition of solid molecular hydrogen, and the smaller feature near 8 meV arises from the solid H_2 translational modes. The spectra at higher temperatures are reflective of the phase change from solid H_2 to liquid H_2.

The long-range diffusive behaviour of H indicated by the elastic peak at the higher temperatures strongly suggests that we are dealing with *bulk liquid* H_2 (*i.e.* an agglomeration of H_2 molecules); the motions of trapped single H_2 molecules would most likely not be 'long-ranged'. Also the inelastic features at 6 K near 8 meV (H_2 translational modes) and near 14 meV (*ortho–para* H_2 rotational transitions) are strongly suggestive of *bulk solid* H_2. This would suggest that the H_2 molecules are concentrated in bubbles and are not in the bulk as isolated H_2 molecules. It is also known that while vacancy trapping is substantially stronger in the transition metals Fe and Ni, H_2 bubble formation is favoured in Al, with a binding enthalpy of 0.71 eV compared to 0.52 eV (Myers *et al.*, 1989). Studies of the solubility of H in metals, and in particular in Al, show that it is present as interstitial H atoms and that there are negligible concentrations of molecular H_2 (Ransley & Neufeld, 1948; Ichimura *et al.*, 1988; Lin & Hoch, 1989; Ichimura *et al.*, 1992; Ichimura & Sasajima, 1993). Since the INS experiment indi-

Table 1
Lattice parameter measurements for samples charged using the gas plasma method compared with uncharged samples.

Within experimental error, $\delta a/a_0$ for foils C and D are equal to a zero change in lattice parameter. The calculated $(\delta a/a_0)_{\text{H only}}$ designates the relative change in lattice parameter (expansion) given that the H enters the lattice interstitially.

Sample	H/M (a.p.p.m.)	a ($\pm 8 \times 10^{-6}$ nm)	$\delta a/a_0$ ($\pm 5 \times 10^{-5}$)	Calculated $(\delta a/a_0)_{\text{H only}}$
Foil D: uncharged Al foil (purity 98.6%)	160	0.404914		
Foil D: Al foil (98.6% pure; t = 65 h; J = 0.57 mA cm^{-2})	1300	0.404898	-4×10^{-5}	7.6×10^{-5}
Foil C: uncharged Al foil (purity 99.99%; thickness 130 μm)	460	0.405028		
Foil C: Al foil (99.99% pure; t = 75.65 h; J = 0.68 mA cm^{-2})	2880	0.405031	7×10^{-6}	1.68×10^{-4}

cates that after charging, H is present as H_2 molecules, we conclude that the bubbles shown in Figs. 6 and 7 are bubbles that contain molecular H_2.

The volume concentration of vacant sites (C_v) was determined from precision density measurements and the result $3.3 \times 10^{-2} \pm 1.0 \times 10^{-2}$ was, within experimental error, equal to C_v calculated from the SANS and USANS experiments (Buckley *et al.*, 1999). It is assumed that the volume of the bubbles is formed from the vacancies created by the initial 1 keV ions, hence $C_v = C_b$, the volume concentration of bubbles. Although Figs. 6–11 show unambiguous evidence that H_2 bubbles are in the bulk and on the surface of the Al foil, there is no evidence that the bubbles are homogeneously distributed in the sample. In fact it was found that certain regions of foil C were preferentially hydrided compared with other regions. Inspection of the foils after charging showed the surface of the foils to be inhomogeneously coloured (dark and light regions), indicating regions of high and low concentrations of H. This was verified by measuring the H concentration (using gas chromatography) on two halves of a foil, which had been plasma charged under the same conditions as foil C. A higher H concentration was measured for the portion of foil which contained predominantly darker regions. Hence the H concentration of foil C (2880 a.p.p.m.) is an average value, with the darker regions of the foil containing a higher H concentration and the lighter regions having a lower concentration than the average value. A darker region of foil C (2×2 cm portion of the sample) was chosen for the X-ray diffraction measurement to ensure that the relative change in lattice parameter was measured on a hydrided region of foil C containing an H concentration of at least 2880 a.p.p.m.

Evidence for the bubbles being distributed inhomogeneously throughout the sample can be found in the slope at low q, of -4.27, from the SANS measurements (see Fig. 5). Schmidt (1991) showed that for a porous material, when the density change at the surface is not sharp, but instead is continuous, the scattering intensity decreases more rapidly than with q^{-4}. In our experimental situation the porous material can be represented by the H bubbles/vacancies in Al, and the density change at the surface will be caused by the diffusion of vacancies and the formation and migration of H–vacancy complexes. The decrease in slope is steeper than expected (<-4) because the interface between the micrometre-size H bubbles and Al is not sharp, but instead is interlaced with a variety of smaller bubbles (see Fig. 7) resulting from the competing processes of the diffusion of H–vacancy complexes and the plasma bombardment of H ions. The slope of -4.27 in the low-q region of the SANS experiment points to the bubbles being inhomogeneously distributed throughout the sample.

In the following analysis, the integrated intensity Q_0, the relative change in lattice parameter $\delta a/a_0$, the average pressure in the bubbles p, the volume concentration of bubbles C_b, and the ratio of the number of vacancies to the number of H atoms, are calculated from the SANS and USANS data. The results for $\delta a/a_0$ and C_b are compared with the experimental results.

The pressure of the H_2 gas in a spherical bubble of volume $\bar{V}_b$ will cause a relative change in the lattice parameter given by (Hirth & Lothe, 1968)

$$\delta a/a_0 = (C_d/3)[(3B + 4\mu)/3B](\bar{V}_b/B)p, \qquad (1)$$

where C_d is the number of bubbles per unit volume, B is the bulk modulus (77 GPa for Al), μ is the shear modulus (26.5 GPa for Al), $\bar{V}_b$ is a bubble of average volume, and p is the pressure of a bubble of average volume. It is important to note that in (1), $\delta a/a_0$ is calculated from the pressure in a bubble of average volume. The experimental value for $\delta a/a_0$ can be compared with that calculated from (1) because the experimentally determined relative change in lattice parameter is an average value. C_b can be expressed as

$$C_b = C_v = V_{\text{vt}}/V = N_v v_{\text{vac}}/V = V_{\text{bt}}/V = C_d \bar{V}_b, \qquad (2)$$

where V is the volume of the irradiated portion of the sample, V_{vt} is the total volume of vacant sites and V_{bt} is the total volume of bubbles. Equation (1) can now be written in the form

$$\delta a/a_0 = pC_b(3B + 4\mu)/(3B)^2. \qquad (3)$$

A lower limit of C_b can be determined from the SANS and USANS data by calculating the integrated intensity (Q_0) of the two sets of data and relating it to C_b. Note that Q_0 is calculated from a combination of SANS and USANS data including the extrapolated region between the two data sets (see dashed line in Fig. 2). Since $C_b \ll 1$, Q_0 is given by (*e.g.* Epperson *et al.*, 1974)

$$Q_0 = 2\pi^2 \Delta\eta^2 C_b = \int_0^\infty I(q) q^2 \, \mathrm{d}q, \qquad (4)$$

where $\Delta\eta$ is the scattering-length density difference between the matrix and the particle given by $\Delta\eta = \eta_B - \eta_{\text{Al}}$, where $\eta_B = N_{\text{H}} b_{\text{H}}/N_V v_{\text{vac}}$ and $\eta_{\text{Al}} = b_{\text{Al}}/v_{\text{Al}}$. η_B is the scattering-length density of the bubble, η_{Al} is the scattering-length density of Al,

b_{Al} is the scattering length of Al (0.3446×10^{-12} cm), b_H is the scattering length of H (-0.3740×10^{-12} cm), N_H is the number of H atoms, N_V is the number of vacancies, v_{vac} is the relaxed atomic volume of a vacancy, v_{Al} is the atomic volume of Al (1.66×10^{-23} cm^3) and $v_{vac} = 0.65 v_{Al}$ (Seeger, 1973). The SANS, USANS, SEM, TEM and INS results are consistent with a large distribution of bubble sizes with radii of approximately 2 nm to 12.1 μm. Therefore, η_B will not be a constant, but in reality will be pressure dependent (Carsughi, 1994). However, we are interested in calculating $\delta a/a_0$, and comparing it with the experimental value, which is an average value and hence independent of the pressure distribution. Therefore, the assumption of a constant contrast should be a reasonable approximation.

The total volume of irradiated sample can be expressed by

$$V = v_{Al} N_m + N_b \bar{V}_b, \tag{5}$$

where N_b is the number of bubbles, $N_m = N_H/C_H$ is the number of metal atoms in the sample and C_H = 2100 a.p.p.m., measured using the PGAA technique (Lindstrom *et al.*, 1993), is the concentration of H atoms in the sample. From (5) the number of H atoms per average bubble volume is

$$N_H/\bar{V}_b = N_b C_H (1 - C_b)/C_b v_{Al}. \tag{6}$$

Therefore

$$n_{H_2}/\bar{V}_b = (1 - C_b) C_H / 2 C_b v_{Al} A_v, \tag{7}$$

where n_{H_2} is the number of moles of H_2 per bubble and A_v is Avogadro's number (6.022×10^{23} atoms mol^{-1}). From (6) and (2), the ratio of the number of H atoms to vacancies can be determined:

$$N_H/N_V = (1 - C_b) C_H v_{vac}/C_b v_{Al}. \tag{8}$$

Since N_H/N_V is not known, C_b is found by rearranging (4) and the expressions for $\Delta\eta$, and substituting (8) into the expression for η_B, resulting in C_b being the solution to a quadratic equation,

$$\alpha C_b^2 + \beta C_b + \zeta = 0, \tag{9}$$

where

$$\alpha = (2\pi^2 C_H^2 b_H^2 + 4\pi^2 C_H b_H b_{Al} + 2\pi^2 b_{Al}^2)/v_{Al}^2, \tag{10}$$

$$\beta = (-4\pi^2 C_H^2 b_H^2 - 4\pi^2 C_H b_H b_{Al})/v_{Al}^2 - Q_0 \tag{11}$$

and

$$\zeta = 2\pi^2 C_H^2 b_H^2 / v_{Al}^2. \tag{12}$$

The pressure of H_2 in a bubble of average volume is calculated by substituting (7) into the Virial equation

$$P = n_{H_2} RT/\bar{V}_b + B_1(T) n_{H_2}^2 RT/\bar{V}_b^2 + B_2(T) n_{H_2}^3 RT/\bar{V}_b^3, \tag{13}$$

where R is the gas constant (8.3144 J K^{-1} mol^{-1}), T is the temperature (K), $B_1(T) = 8.14 \times 10^{-11} T^2 + 7.28 \times 10^{-8} T + 1.03 \times 10^{-6}$ and $B_2(T) = -1.0 \times 10^{-12} T + 6.9 \times 10^{-10}$ (Dymond & Smith, 1969). Since the second and third term in (13) are 3.62% and 0.25% of the total pressure, they can be neglected and hence the ideal gas equation can be used. Finally, $\delta a/a_0$ is calculated by substituting p from (13) and C_b into (3).

Table 2 represents a comparison between the experimental and the calculated values of $\delta a/a_0$ and C_b, and also lists the calculated values of the pressure in a bubble of average volume and the number of vacancies per H atom, N_v/N_H. The experimental and calculated values of C_b and N_v/N_H, and the calculated pressure are determined for foil B (C_H = 2100 a.p.p.m. and $C_b = 3.3 \times 10^{-2}$ from precision density measurements). The experimental value of $\delta a/a_0$ is determined for foil C, and $\delta a/a_0$ is calculated for foils C (C_H = 2880 a.p.p.m.) and B (C_H = 2100 a.p.p.m.). Since the values of C_H for foils B and C are similar, it is assumed that C_b for foil C will also be $\ll 1$ (as is the case for foil B) and therefore the calculation of $\delta a/a_0$ will be independent of C_b [substitute equation (7) into (13) and the first term of (13) into (3)] for both foils B and C. Hence an experimental measurement of C_b was not required to calculate $\delta a/a_0$ for foil C. The error in the calculated values of $\delta a/a_0$ comes from the experimental errors in C_H, μ, B, T and v_{Al}, and the main source of error in the calculated values of C_b, p and N_v/N_H is the calculation of Q_0 [see equation (4)], which is derived from the experimental SANS and USANS data. The experimental and calculated values of $\delta a/a_0$ are within experimental error equal to zero, and this result agrees with the hypothesis that hydrogen does not enter the lattice interstitially, but instead forms an H–vacancy complex at the surface, which diffuses into the volume and then clusters to form H_2 bubbles. The calculated value of C_b is within experimental error equal to the precision density measurement. The low value for the calculated average molecular pressure is also consistent with the formation of bubbles by the clustering of H–vacancy complexes (Condon, 1993).

It is stressed that the calculated pressure is the pressure in a bubble of average volume. The SANS, USANS, INS, TEM and SEM results indicate that the hydrided samples contain a large distribution of bubble sizes with radii of approximately 1 nm to 12.1 μm, resulting in a pressure distribution of approximately 0.1 MPa to 1.72 GPa. This distribution is calculated from $p = 2\gamma/r$, where r is the radius of a spherical bubble and γ = 0.86 Nm^{-1} is the surface tension of Al. Since the experimental value of $\delta a/a_0$ is an average value, it will be independent of the true pressure distribution; therefore the method of calculating $\delta a/a_0$ need only rely on an expression which is dependent on a pressure in a bubble of average volume [see equations (3) and (13)]. The agreement between experimental and calculated values of $\delta a/a_0$ indicates that the calculation of the pressure in a bubble of average volume is a reasonable assumption.

The large value of N_V/N_H = 30 is also indicative of a low average molecular pressure. For every H atom that diffuses into the bulk with a vacancy, on average 30 vacancies are created. The H_2 bubbles are formed by H–vacancy complexes clustering together with the resulting internal pressure being relieved by the compressive field of the H_2 bubbles attracting extra vacancies created by the initial 1 keV

Table 2
Comparison of experimental and calculated values for $\delta a/a_0$ and C_b.

Also shown are the calculated values for the pressure of a bubble of average volume and N_V/N_H for foil B. The calculated and experimental values of C_b and N_V/N_H were determined for foil B and the experimental values of $\delta a/a_0$ were determined for foil C. $\delta a/a_0$ has also been calculated for foils B and C.

	C_b	P (MPa)	$\delta a/a_0$	N_V/N_H
Experiment	$(3.3 \pm 1.0) \times 10^{-2}$ (foil B)	–	$7 \times 10^{-6} \pm 5 \times 10^{-5}$ (foil C)	25 ± 8 (foil B)
Calculation	$(3.9 \pm 0.3) \times 10^{-2}$ (foil B)	6.44 ± 0.60 (foil B)	$(2.3 \pm 0.2) \times 10^{-6}$ (foil C) $(1.7 \pm 0.2) \times 10^{-6}$ (foil B)	30 ± 3 (foil B)

ions. The additional vacancies are probably created near the surface by the H^+ ion impacts (see Fig. 1).

The calculation of $\delta a/a_0$ and p does *not* rely on a knowledge of the average volume of the bubble. The important parameter is $n_{H_2}/\bar{V}_b$. The above method allows one to calculate p and hence $\delta a/a_0$ without having to determine $\bar{V}_b$ from the radial or volume distribution functions calculated from the SANS and USANS data. The wide distribution of bubble sizes and the fact that the contrast will be size dependent (Carsughi, 1994) makes the task of calculating an accurate and unambiguous size distribution of the bubbles from a combination of the SANS and USANS data an extremely difficult one. The distribution function for the SANS data was calculated (Buckley *et al.*, 1999) using the termination corrector method (Brill *et al.*, 1968; Brill & Schmidt, 1968) and the recurrence numerical corrector method (Mulato & Chambouleyron, 1996). Both methods employed the analytical expression of Fedorova & Schmidt (1978) for the distribution of hard spheres. The recurrence numerical corrector method was also modified by incorporating smearing effects (Barker & Pederson, 1995) into the algorithm. The distribution functions calculated by both methods returned a poor fit to the experimental SANS data, and were not consistent with the TEM and SEM results. The calculation of $\delta a/a_0$ in the present work does not require knowledge of the SANS and USANS distribution function since we are only interested in calculating an average experimental quantity. However, work is in progress to calculate a distribution function for the SANS data using the indirect transform method (Svergun *et al.*, 1988) and the maximum-entropy method (Potton *et al.*, 1988). The distribution function for Fig. 2 could then be determined and compared with data from further TEM work, which is in progress.

4. Conclusions

Results from initial SAXS experiments on Al single crystals that were cathodically charged with hydrogen suggested scattering from platelet-shaped inhomogeneities habitating the {111} or {112} planes. However, this scattering could not be distinguished from DBS; therefore to eliminate the DBS, a SANS experiment using $\lambda = 0.8$ nm (*i.e.* $\lambda > \lambda_c$) was conducted on polycrystalline Al samples that were plasma-charged with hydrogen. The SANS and USANS experiment revealed scattering from a wide distribution of particle sizes and the SANS data suggested that the scattering was unlikely to be from platelet-shaped inhomogeneities. Further investigations using INS, TEM and SEM indicated that the scattering is from a large size distribution of hydrogen bubbles. These experiments coupled with X-ray diffraction measurements indicate that hydrogen does not enter the Al lattice interstitially, but instead couples to a vacancy at the surface and diffuses into the bulk; then the H–vacancy complexes cluster together to form hydrogen bubbles. The pressure in a bubble of average volume was calculated and from this result $\delta a/a_0$ was calculated. It is found that within experimental error the calculated $\delta a/a_0$ is equal to that determined experimentally from X-ray diffraction. The H_2 bubbles grow by accretion of vacancies to reduce the strain energy, resulting in approximately 30 vacancies per H atom.

The research undertaken at The University of Illinois was sponsored by the US Department of Energy grant DEFG02-96ER45439, and the research component undertaken at Curtin University was funded by a Curtin University Post Doctoral Research Fellowship. The SAXS research at Oak Ridge was sponsored in part by the US Department of Energy under contract No. DE-AC05-00OR22725 with the Oak Ridge National Laboratory, managed by the UT-Battelle, LLC. The authors would also like to thank John Barker, Jack Rush and Rick Paul from The National Institute of Standards and Technology (NIST) for the SANS, INS and PGAA experimental results.

References

Barker, J. G. & Pedersen, J. S. (1995). *J. Appl. Cryst.* **8**, 105–114.
Bellmann, D., Klatt, M., Kampmann, R. & Wagner, R. (1998). *Physica B*, **241–243**, 71–73.
Birnbaum, H. K., Buckley, C. E., Zeides, F., Sirois, E., Rozenak, P., Spooner, S. & Lin, J. S. (1997). *J. Alloys Compd.* **253–254**, 260–264.
Brill, O. L. & Schmidt, P. W. (1968). *J. Appl. Phys.* **39**, 2274–2281.
Brill, O. L, Weil, C. G. & Schmidt, P. W. (1968). *J. Colloid Interface Sci.* **27**, 479–492.
Buckley, C. E. & Birnbaum, H. K. (1998). *Physica B*, **241–243**, 344–346.
Buckley, C. E. & Birnbaum, H. K. (2000). *J. Alloys Compd.* In the press.
Buckley C. E., Birnbaum, H. K., Bellmann, D. & Staron, P. (1999). *J. Alloys Compd.* **292–293**, 231–236.
Carsughi, F. (1994). *J. Appl. Cryst.* **27**, 326–329.
Condon, J. B. & Schober, T. (1993). *J. Nucl. Mater.* **207**, 1–24.
Copley, J. R. D. & Udovic, T. J. (1993). *J. Res. Natl Inst. Stand. Technol.* **98**, 71–87.
Dymond, J. H. & Smith, E. B. (1969). *The Virial Coefficients of Gases: a Critical Compilation*. Oxford: Clarendon.
Epperson, J. E., Hendricks, R. W. & Farrell, K. (1974). *Philos. Mag.* **30**, 803–817.

Fedorova, I. S. & Schmidt, P. W. (1978). *J. Appl. Cryst.* **11**, 405–411.
Hirth, J. P. & Lothe, J. (1968). *Theory of Dislocations*. New York: McGraw-Hill.
Ichimura, M., Katsuta, H., Sasajima, Y. & Imabayashi, M. (1988). *J. Phys. Chem. Solids*, **49**, 1259–1267.
Ichimura, M. & Sasajima, Y. (1993). *Mater. Trans. JIM*, **34**, 404–409.
Ichimura, M., Sasajima, Y. & Imabayashi, M. (1992). *Mater. Trans. JIM*, **33**, 449–453.
Ishikawa, T. & Mclellan, R. B. (1986). *Acta Metall.* **34**, 1091–1095.
Kamada, K. (1989). *J. Nucl. Mater.* **169**, 141–150.
Kamada, K., Sagara, A., Kinoshita, H. & Takahashi, H. (1987). *Radiat. Eff.* **103**, 119–133.
Kamada, K., Sagara, A., Kinoshita, H. & Takahashi, H. (1988). *Radiat. Eff.* **106**, 219–227.
Lin, R. Y. & Hoch, M. (1989). *Metall. Trans. A*, **20A**, 1785–1791.
Lindstrom, R. M. (1993). *J. Res. Natl Inst. Stand. Technol.* **98**, 127–133.
Milacek, L. H. & Daniels, R. D. (1968). *J. Appl. Phys.* **39**, 5714–5717.
Mulato, M. & Chambouleyron, I. (1996). *J. Appl. Cryst.* **29**, 29–36.
Myers, S. M., Richards, P. M., Wampler, W. R. & Besenbacher, F. (1989). *J. Nucl. Mater.* **165**, 9–64.
Peisl, H. (1978). *Hydrogen in Metals I, Topics in Applied Physics*, Vol. 28, edited by G. Alefeld & J. Volkl, pp. 53–74. Berlin: Springer.
Porod, G. (1951). *Kolloid-Z.* **124**, 83–114.
Potton, J. A., Daniell, G. J. & Rainford, B. D. (1988). *J. Appl. Cryst.* **21**, 663–668.
Ransley, C. E & Neufeld, H. (1948). *J. Inst. Met.* **74**, 599–620.
Russell, T. P., Lin, J. S., Spooner, S. & Wignall, G. D. (1988). *J. Appl. Cryst.* **21**, 629–668.
Schelten, J. & Schmatz, W. (1980). *J. Appl. Cryst.* **13**, 385–390.
Schmidt, P. W. (1991). *J. Appl. Cryst.* **24**, 414–435.
Seeger, A. (1973). *J. Phys. F Met. Phys.* **3**, 248–294.
Staron, P. & Bellmann, D. (2001). *J. Appl. Cryst.* Submitted.
Svergun, D. I., Semenyuk, A. V. & Feigin, L. A. (1998). *Acta Cryst.* A**44**, 244–250.
Wei, L. X., Ruault, M. O., Traverse, A. & Bernas, H. (1987). *J. Less-Common Met.* **130**, 133–138.
Wignall, G. D., Lin, J. S. & Spooner, S. (1990). *J. Appl. Cryst.* **23**, 241–245.
Ziegler, J. F., Biersack, J. P. & Littmark, U. (1985). *The Stopping and Range of Ions in Solids*, edited by J. F. Ziegler, pp. 109–126. New York: Pergamon.